

Amino-Acid Side-Chain Nanoarchitectonics for Tuning the Chiroptical Properties and Supramolecular Structure of Pentameric Oligothiophenes

Linnea Björk,^[a] Robert Selegård,^[b] Marcus Bäck,^[a] Per Hammarström,^[a] Mikael Lindgren,^[c] and K. Peter R. Nilsson^{*[a]}

Oligothiophenes with specific photophysical properties and molecular organization are of great interest, since this class of materials are used in organic electronics and bioelectronics, as well as biosensing. Herein, 8 different pentameric oligothiophenes, denoted proteophenes, with different amino acid substitution patterns at distinct positions along the thiophene backbone were investigated. Spectroscopic and microscopic studies of the ligands revealed the formation of optically active self-assembled materials under acidic or basic conditions. The distinct photophysical characteristics, including induced circular dichroism, as well as the supramolecular structures of the assemblies deduced from light scattering and transmission electron microscopy, were highly influenced by the positioning

of distinct amino acid moieties along the thiophene backbone. Proteophenes functionalized with only glutamate residues or these functionalities in combination with hydrophobic valine moieties formed fibrillar structures with excellent chiroptical properties under acidic conditions. In addition, the amino acid functionality at the β -position of distinct thiophene moieties influenced the induced circular dichroism pattern observed from the proteophenes. Overall, the obtained results demonstrate how changes in the position of various amino acid functionalities, as well as the chemical nature of the amino acid side chain functionality greatly affect the optical properties as well as the architecture of the self-assembled materials.

Introduction

Chiral optoelectronic materials comprised of conjugated poly- and oligothiophenes (CPs and COs) that exhibit optical activity in the π - π^* transition region are widely explored for organic and bioelectronics, since these materials can be utilized for a variety of applications, such as optoelectronic devices, biosensors, and as artificial enzymes.^[1–13] Optical activity has frequently been observed from CPs functionalized with an optically active substituent in the 3-position and an induced circular dichroism (ICD) is afforded when the polymer chains are

forming supramolecular assemblies in poor solvents or at low temperature.^[5,14–17] Moreover, a single chain ICD has also been obtained from optically inactive CPs and COs when mixed with small chiral molecules or synthetic peptides,^[9–11,18–22] as well as for CPs with L- or D-amino acid side chain functionalities along the conjugated thiophene backbone.^[23,24] For the latter, the configuration of the amino acid, L- or D-form, created right-handed or left-handed helical forms of the polythiophene chains with distinct ICD patterns.^[24]

A correlation between the chemical composition of the material and the ICD patterns have also been reported for chemically defined oligothiophenes having specific chiral substituents at different positions along the oligothiophene backbone.^[25–32] A diversity of penta(ethyleneoxide) functionalized oligothiophenes displayed distinct aggregation induced Cotton effects and the different ICD patterns could be correlated to the position of the chiral substituent as well as the length of the oligothiophene backbone.^[26] Likewise, oligothiophenes functionalized with different sugar moieties or amino acids showed specific ICD patterns, helicity and structural organization that could be linked to the configuration, as well as the position of the chiral substituent.^[27,28,32] Hence, distinct enantiomeric substitutions at specific position along the conjugated oligothiophene backbone can be utilized to tune the optical activity, as well as the self-assembly of chemically defined oligothiophenes.

Herein we investigated the chiroptical properties and supramolecular arrangement of a set of anionic pentameric oligothiophenes having different amino acids introduced at distinct positions along the conjugated backbone (Figure 1).

[a] L. Björk, Dr. M. Bäck, Prof. P. Hammarström, Prof. K. P. R. Nilsson
Division of Chemistry, Department of Physics, Chemistry and Biology
Linköping University
581 83 Linköping (Sweden)
E-mail: peter.r.nilsson@liu.se

[b] Dr. R. Selegård
Division of Biophysics and Bioengineering, Department of Physics,
Chemistry and Biology
Linköping University
581 83 Linköping (Sweden)

[c] Prof. M. Lindgren
Department of Physics,
Norwegian University of Science and Technology
7491 Trondheim (Norway)

Supporting information for this article is available on the WWW under <https://doi.org/10.1002/cptc.202300183>

© 2023 The Authors. ChemPhotoChem published by Wiley-VCH GmbH. This is an open access article under the terms of the Creative Commons Attribution Non-Commercial License, which permits use, distribution and reproduction in any medium, provided the original work is properly cited and is not used for commercial purposes.

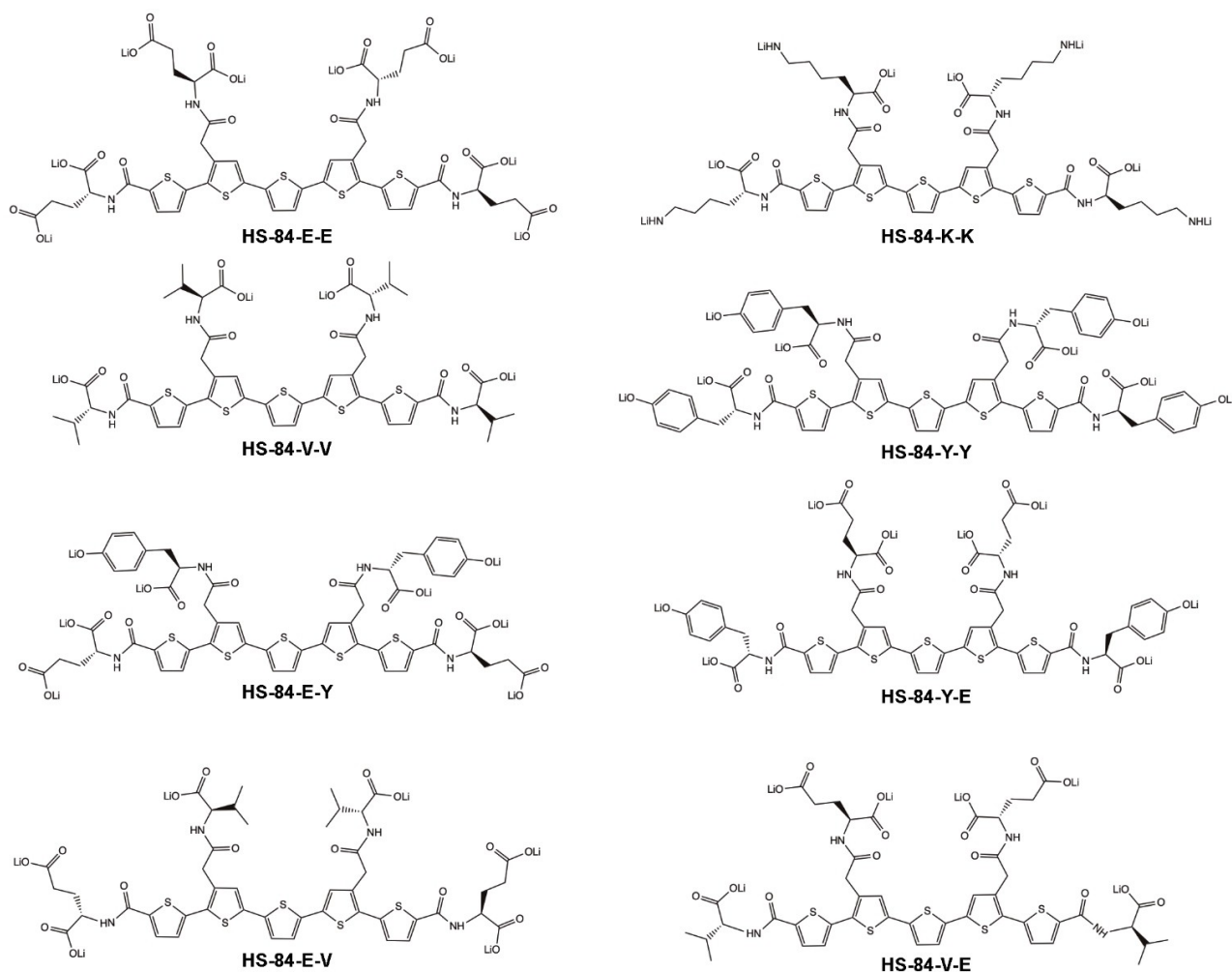


Figure 1. Chemical structures of different pentameric proteophenes with specific amino acid side functionalities along the conjugated backbone. All the proteophenes were isolated as the Li-salt and in acidic conditions (pH 2) all the carboxyl and the amine groups, as well as the phenolic hydroxy groups of the ligands should predominantly be protonated, whereas in alkaline conditions (pH 10) all these chemical groups should be mainly deprotonated.

These ligands, denoted proteophenes, were recently shown to exhibit differential binding to aggregated proteinaceous species in human brain tissue samples with Alzheimer's disease (AD) pathology.^[33] The proteophenes have specific amino acid residues introduced at the β -position of distinct thiophene moieties and at the terminal α -positions of the oligothiophene backbone and the effects of these structural modifications on the chiroptical properties and supramolecular arrangement of the respective ligand were assessed by comparing the photo-physical characteristics and self-assembling properties of the chiral proteophenes under acidic (pH 2) or basic (pH 10) conditions. The obtained results revealed that the chemical nature, as well as the position of the amino acid substituents, have a large impact on the proteophenes optical properties and the molecular architecture of the self-assembled structures.

Results and Discussion

Absorption and Emission Characteristics

The synthesis of the proteophenes (Figure 1) has been reported previously.^[33] To assess the photo-physical characteristics of the amino acid functionalized oligothiophenes, the ligands were dissolved in two different buffer solutions, 10 mM Na-Citrate pH 2 or 10 mM Na-carbonate pH 10, respectively. These buffers were selected, since earlier studies have shown that pH-induced conformational changes of the thiophene backbone can be afforded for both anionic oligo- and polythiophenes.^[34–38] Furthermore, in acidic conditions (pH 2) all the carboxyl- and amine groups of the proteophenes should predominantly be protonated, whereas in alkaline conditions, the carboxyl groups, as well as the phenolic hydroxy groups and amine groups should be deprotonated. In 10 mM Na-carbonate pH 10, all the proteophenes, displayed similar absorption spectra with a maximum between 418 nm to 430 nm (Figure 2, Supporting information, SI, Table S1). The emission maxima in alkaline

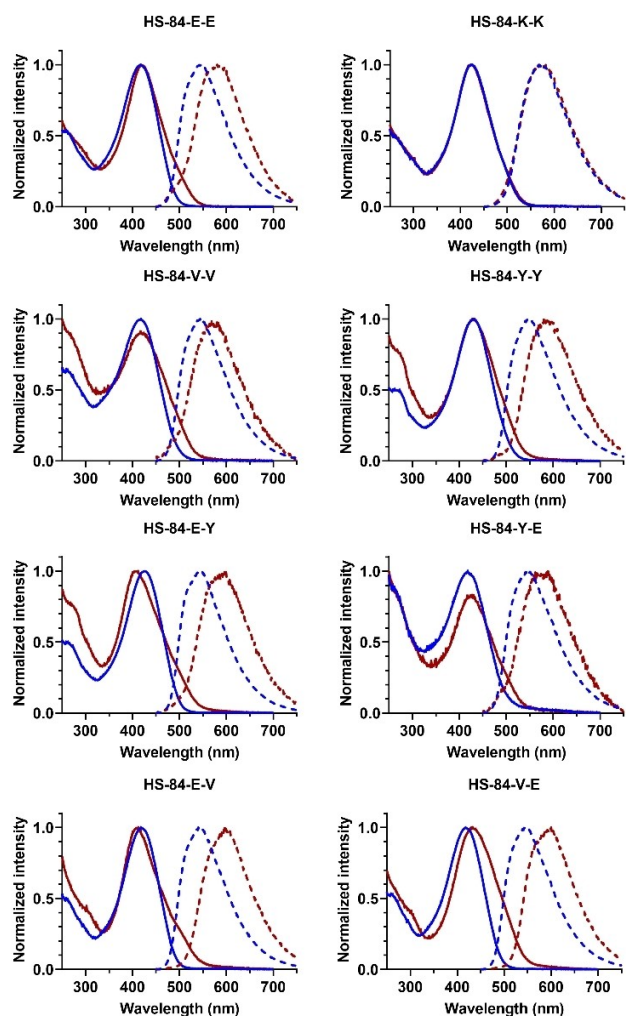


Figure 2. Photophysical characteristics of different pentameric proteophenes in acidic or alkaline conditions. Absorption- (solid lines) and emission (dotted lines) spectra of 50 μM proteophene diluted in 10 mM Na-Citrate pH 2 buffer (red lines) or 10 mM Na-carbonate pH 10 buffer (blue lines). Emission spectra was collected with the excitation wavelength correlated to the absorption maximum for the respective proteophene.

condition were all comparable for all ligands (541 nm to 548 nm) except for HS-84-K-K that display a red-shifted emission maximum at 575 nm (Figure 2 and SI, Table S1). These photophysical characteristics are similar to the ones reported for other anionic pentameric oligothiophenes in neutral or alkaline conditions,^[33–37] suggesting that the absorption- and emission spectra from the proteophenes in 10 mM Na-carbonate pH 10 buffer originates from fully dissolved single oligothiophene chains or tiny clusters of chains with high resemblance of the ground and excited electronic states of the substituted variants. In 10 mM Na-citrate pH 2 buffer, HS-84-K-K showed analogous optical characteristic as in alkaline conditions, whereas the other proteophenes showed distinct different absorption- and emission characteristics in alkaline or acidic conditions (Figure 2, SI Table S1). HS-84-E-E, HS-84-V-V, HS-84-Y-Y showed similar absorption maxima in the two conditions, but in acidic conditions, an additional shoulder at longer wave-

lengths was observed for all the ligands. A similar shoulder was also detected for HS-84-E-Y, HS-84-Y-E, HS-84-E-V and HS-84-V-E, but these ligands also displayed an additional blue-shift (HS-84-E-V and HS-84-E-Y) or red-shift (HS-84-Y-E and HS-84-V-E) of the absorption maximum (Figure 2, SI, Table S1). A red-shift of the emission spectra in acidic conditions was also observed for all the ligands except for HS-84-K-K and this shift is most likely associated with a planarization of the backbone that are induced upon protonation of the carboxyl groups.^[23,39–42] Moreover, in acidic conditions, the emission intensity decreased with one to two orders of magnitude, suggesting an aggregation of adjacent oligothiophene molecules (SI, Figure S1).^[15–17,23] The decrease in emission in acidic condition was lacking for HS-84-K-K, suggesting that this ligand display fully dissolved single oligothiophene chains in both the conditions.

In general, the photophysical assessment established that the chemical nature of the amino acid side chain functionalities and variations in the position of these chemical moieties along the conjugated thiophene backbone have a considerable impact on the proteophenes optical behaviour. In addition, the ligands presumably form different types of molecular arrangements or aggregates in the different buffer solutions. For COs and CPs, a red-shift of the main absorption peak are normally associated with J-aggregates, whereas a blue-shift is related to the formation of H-aggregates.^[43–46] Thus, in line with the absorption data (Figure 2), HS-84-Y-E and HS-84-V-E most likely form J-aggregates in pH 2 buffer, whereas H-aggregates seem to be formed for HS-84-E-V and HS-84-E-Y in the same conditions. Nevertheless, a red-shifted absorption can also be a consequence of other molecular re-arrangements, such as planarization of the conjugated oligothiophene backbone.^[23,39–42] For instance, the anionic pentameric oligothiophene, penta formyl thiophene acetic acid (p-FTAA), were shown to form H-aggregates in acidic conditions regardless of a pH-induced red-shift of the absorption maximum.^[38] A recent study of pentameric oligothiophenes functionalized with L- or D-tyrosine residues also showed that the location of the amino acid functionalities of the oligothiophene backbone had a great impact on the optical behaviour of the ligands, as ligands having tyrosine residues in the β -positions showed a greater pH-induced red-shifted absorption maximum compared to a ligand with tyrosine functionalities at the terminal α -positions.^[32] Interestingly, when comparing HS-84-Y-Y with the previously reported p-FTAA-L-Tyr (SI, Figure S2), similar absorption and emission characteristics were obtained for both ligands in buffer pH 2, whereas in alkaline conditions (buffer pH 10) a slightly red-shifted absorption maximum and a blue-shifted emission spectrum were observed for HS-84-Y-Y (SI, Figure S2). From a chemical perspective, these ligands have both tyrosine functionalities at the terminal α -positions, but p-FTAA-L-Tyr is lacking the amino acid functionalities in the β -position of the thiophene moieties surrounding the central thiophene unit.

Next, the quantum yield (QY) of the emitted light from the respective proteophene was assessed. In addition to the two buffer solutions, pH 2 and pH 10, methanol was used as a reference 'good solvent', along with Coumarin 153 as QY reference.^[47] These reference QYs were measured using

standard 3 mL 1 cm path quartz cuvettes. Representative spectral results and slope plots^[47] are shown in Figure S3 and S4. As the results implied aggregation at the low and/or high pH that might change over time, the QY for pH 2 and pH 10 was estimated from defined single point measurements. In this regard, a fresh sample was made by first ultrasonicate the stock solution (1.5 mM) and diluted to 5 μ M using smaller cuvettes (500 μ L; 5 mm path). To obtain the QY, the emission was integrated and normalized to the absorption at the excitation wavelength (455 nm). The calculated QYs are summarized in Table 1. Conclusively, the QYs using methanol were around 20% with HS-84-K-K giving the lowest value of 15%, whereas HS-84-E-V gave the highest yield of 24%. In pH 10 buffer the QY was comparable to the methanol results but slightly lower in all cases. A general trend was that the proteophenes having E and V sidechain functionalities gave slightly higher QYs in methanol and pH 10 buffer. In contrast, in pH 2 buffer solution the QY was drastically reduced approximately by an order of magnitude in most cases (Table 1). The HS-84-K-K was found to be an exception with identical QY of 5.9% in both pH 2 and pH 10 buffer. As shown above, the spectral features of this ligand in different pH were also very similar (Figure 2).

The lifetimes of the various proteophenes were also measured and analyzed, using the same samples as prepared for the QY characterization. Here time-correlated single photon (TC-SPC) was employed using an excitation wavelength at 455 nm. Representative TC-SPC decays for two of the proteophenes, HS-84-E-E and HS-84-V-V, in pH 2 and pH 10 buffer are shown in Figure S5. Generally, the decay traces were not following a single decay-time model but could be fitted to a 2-component model (solid lines). For HS-84-V-V, in pH 2 buffer the two decay times: $\tau_1 = 57 \pm 6$ ps ($w_1 = 82\%$) and $\tau_2 = 1296 \pm 8$ ps ($w_2 = 18\%$) were afforded, where w_i indicate the normalized amplitude weight. Although the amplitude was much higher for the short component the overall slow appearance of the decay was determined by the much longer decay time since each component contribute with $\tau_i \cdot w_i$ for each component (the integrated area). Likewise, for HS-84-V-V in pH 10 buffer, the decay times $\tau_1 = 358 \pm 18$ ps ($w_1 = 58\%$) and $\tau_2 = 781 \pm 10$ ps ($w_2 = 42\%$) were obtained. Thus, to compare the overall decay, the intensity average was calculated for each multicomponent decay: $\tau_{ave} = \sum_i (w_i \cdot \tau_i^2) / (w_i \cdot \tau_i)$ and the results are summar-

ized in Table 2. In acidic pH most of the ligands showed longer decay features compared to in alkaline pH. The HS-84-K-K and HS-84-Y-Y were exceptions, as the pH 10 cases show a somewhat longer decay time. In MeOH, very similar decay times around 820–840 ps within the experimental uncertainty, were observed for all the proteophenes, again corroborating a similar excited state for all the well dissolved individual molecular configurations. Overall, the quantum efficiency and decay time results supports the general features of the absorbance and emission spectra for the different solvents. There is a clear indication of aggregation both from the drastically reduced QY at acidic pH for some variants, and for the associated decay traces there are components with longer decay times appearing.

Induced Circular Dichroism

To investigate the optical activity of the proteophenes, circular dichroism (CD) measurements of the ligands dissolved in 10 mM Na-Citrate pH 2 buffer or 10 mM Na-carbonate pH 10 buffer were performed. In pH 2 buffer, all the ligands displayed a split-type bisignate ICD in the π - π^* transition region (Figure 3) and these ICDs are most likely associated with π -stacked chiral aggregation of the ligands. Similar aggregation induced ICDs have been observed earlier for chiral oligo- and polythiophenes,^[5,13–17,26–29,32] and the indication of aggregate formation is also supported by the already discussed pH-induced photophysical changes, such as red-shifts in absorption spectra, as well as the decreased emission intensities under acidic condition (Figure 2 and SI, Figure S1). The most pronounced ICDs were obtained for HS-84-E-V, HS-84-E-E and HS-84-V-E, whereas the other proteophenes displayed less intense ICDs (Figure 3) and similar to was reported for chiral polythiophenes,^[15,17] as well as tyrosine functionalized oligothiophenes,^[32] the ICD pattern resembled the first derivative of the absorption spectrum for the respective proteophene (SI, Figure S6). For HS-84-K-K, HS-84-Y-Y and HS-84-E-Y a positive Cotton effect was observed at longer wavelengths, whereas a negative Cotton effect was displayed at shorter wavelengths. In contrast, HS-84-E-E, HS-84-V-V, HS-84-Y-E, HS-

Table 1. Quantum efficiencies of 5 μ M proteophene in Na-Citrate pH 2 buffer, 10 mM Na-Carbonate pH 10 buffer, and methanol (MeOH).

Proteophene	QY MeOH (%)	QY pH 2 (%)	QY pH 10 (%)
HS-84-E-E	22.5 \pm 1.9	2.8	17
HS-84-K-K	14.8 \pm 1.2	5.9	5.9
HS-84-V-V	23.0 \pm 1.8	0.56	21
HS-84-Y-Y	17.3 \pm 1.4	0.92	12
HS-84-E-Y	20.9 \pm 1.7	1.1	18
HS-84-Y-E	20.3 \pm 1.7	2.7	15
HS-84-E-V	24.3 \pm 2.0	1.3	19
HS-84-V-E	23.9 \pm 1.9	2.0	17

Table 2. TC-SPC decay times of the proteophenes (typically 1–5 μ M) in Na-Citrate pH 2 buffer, 10 mM Na-Carbonate pH 10 buffer, and methanol. The tabulated values are intensity averages as explained in the text.

Proteophene	τ_{ave} (ps) MeOH	τ_{ave} (ps) pH 2	τ_{ave} (ps) pH 10
HS-84-E-E	827 \pm 55	1060 \pm 28	636 \pm 39
HS-84-K-K	818 \pm 52	712 \pm 25	975 \pm 31
HS-84-V-V	841 \pm 51	1396 \pm 148	617 \pm 32
HS-84-Y-Y	851 \pm 50	568 \pm 21	661 \pm 26
HS-84-E-Y	842 \pm 48	670 \pm 29	652 \pm 41
HS-84-Y-E	840 \pm 47	966 \pm 25	595 \pm 29
HS-84-E-V	817 \pm 45	921 \pm 26	611 \pm 33
HS-84-V-E	812 \pm 45	900 \pm 25	612 \pm 42

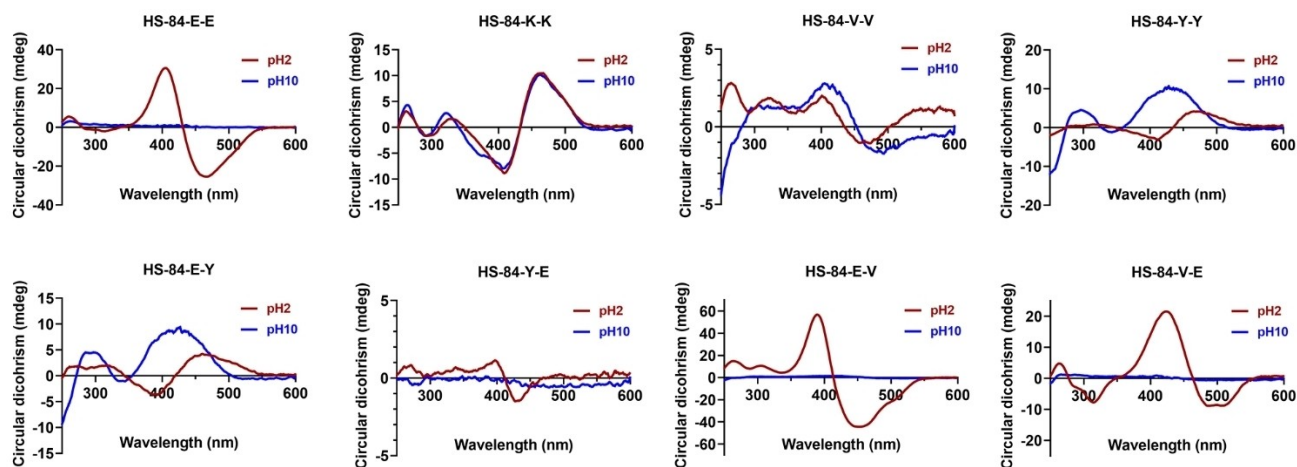


Figure 3. Circular dichroism spectra (CD) of the pentameric proteophenes in acidic or alkaline conditions. CD spectra of 50 μM proteophene diluted in 10 mM Na-Citrate pH 2 buffer (red lines) or 10 mM Na-carbonate pH 10 buffer (blue lines).

84-E-V and HS-84-V-E showed opposite ICD patterns, with a positive Cotton effect at shorter wavelengths and a negative Cotton effect at longer wavelengths, respectively (Figure 3). Thus, both the ICD pattern, as well as the intensity of the ICD, was influenced by the chemical nature of the amino acid side-chain functionalities and the positioning of the amino acid functionality along the conjugated thiophene backbone, verifying that distinct amino acid substitutions along the pentameric oligothiophene backbone had a substantial impact on the helical packing of the thiophene backbone. Similar ICD patterns have also been observed for tyrosine functionalized pentameric oligothiophenes,^[32] as well as for zwitter-ionic polythiophenes having L- or D-serine in the β -positions.^[24] However, for the latter, the ICDs were a result of main-chain chirality instead of aggregation. Recently, mirror images of ICD patterns were also observed in pentameric oligothiophenes with L- or D-tyrosine side-chain functionalities at distinct positions and theoretical calculations indicated that the ICD signals from these ligands originated from conformer populations with distinct dihedral angles between the thiophene rings, as well as an enhancement by the intermolecular chromophore interactions in the formed aggregates.^[32] Oligothiophenes with dihedral angles into the forms of cis-minus (M) showed a positive Cotton effect at higher energy and a negative Cotton effect at low energy, whereas dihedral angles into the forms of cis-plus (P) displayed an opposite ICD pattern.^[32] Thus, the chemical nature of the amino acid side-chain functionalities and the positioning of the amino acid functionality along the conjugated thiophene backbone will most likely influence the dihedral angles between the thiophene rings in different fashion that gives rise to distinct ICD patterns. When comparing the ICD for HS-84-Y-Y in pH 2 buffer with the previously reported p-FTAA-L-Tyr in the same conditions, analogous ICD patterns were observed (SI, Figure S2D), suggesting that these ligands adopt similar molecular organization in acidic conditions.

In alkaline conditions (pH 10), a split-type ICD in the π - π^* transition region was only observed for HS-84-K-K and HS-84-V-V (Figure 3). For HS-84-K-K, the ICD pattern in pH 10 buffer was

in principle identical to the ICD signal in acidic conditions, suggesting that this ligand displays similar conformations in both the conditions, and this is also supported by the photo-physical properties reported above. In contrast, HS-84-V-V, showed a slightly altered ICD pattern in pH 2 buffer compared to alkaline (pH 10) solution. For the latter, the split-type ICD pattern in the π - π^* transition region was slightly shifted towards higher wavelength and in the CD signal in the UV-region, below 300 nm, also showed a negative value whereas a positive sign was obtained for the ligand in acidic conditions (Figure 3). A CD signal was also obtained for HS-84-Y-Y and HS-84-E-Y in alkaline conditions. However, these CD signatures resemble the respective absorption spectra and no split-type bisignate ICD in the π - π^* transition region could be observed (Figure 3). Interestingly, both these ligands, have tyrosine residues in the β -positions of thiophene number 2 and 4, and for the ligands only having tyrosine functionalities in the terminal α -positions, HS-84-Y-E and the previously reported p-FTAA-L-Tyr, observable ICDs in buffer pH 10 were lacking (Figure 3 and SI, Figure S2D). Hence, these signatures were only obtained from proteophenes having tyrosine residues in the β -positions of the oligothiophene backbone.

Dynamic Light Scattering

To further examine if the pentameric oligothiophenes go through a pH dependent structural organization, dynamic light scattering (DLS) measurements were performed in 10 mM Na-Citrate pH 2 buffer or 10 mM Na-carbonate pH 10 buffer. In general, all proteophenes showed analogous scattering intensities and similar lag times in the autocorrelation function in alkaline conditions, as well as hydrodynamic radius, whereas a variation of these parameters between the ligands was observed in acidic conditions (Figure 4, Table 3 and SI, Figure S7). HS-84-E-E, HS-84-K-K and HS-84-Y-E displayed scattering intensities and similar lag times in the autocorrelation function in both conditions (Figure 4 and SI, Figure S7). In contrast, all

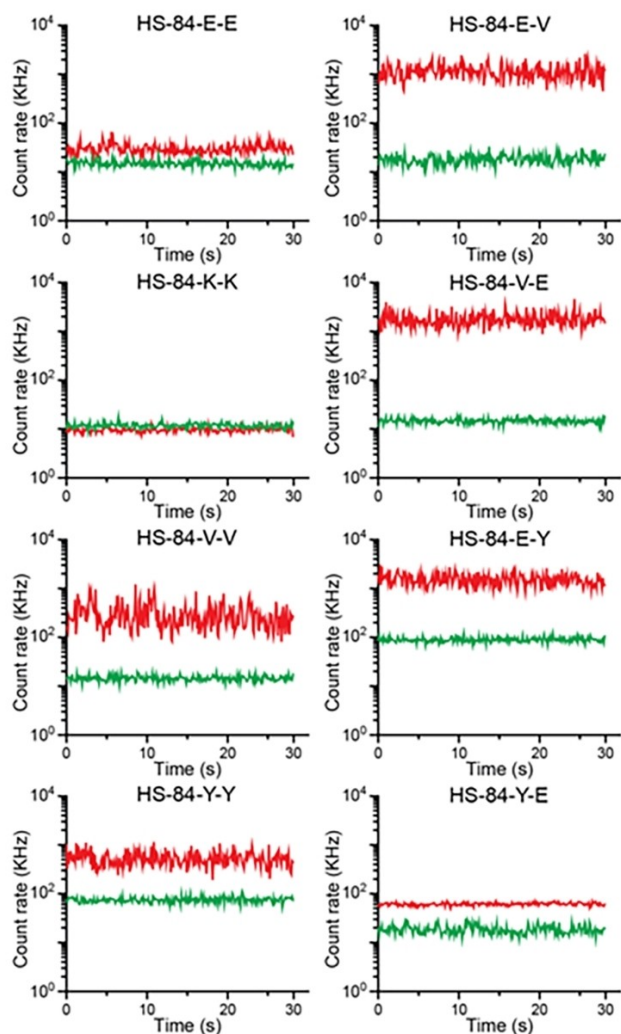


Figure 4. Dynamic light scattering (DLS) measurement of the proteophenes in acidic or alkaline conditions. Scattering intensity recorded by DLS of 50 μ M proteophene in 10 mM Na-Citrate pH 2 buffer (red lines) and Na-Carbonate pH 10 buffer (green lines).

Table 3. Hydrodynamic radius derived from DLS measurements of 50 μ M proteophene in 10 mM Na-Citrate pH 2 or 10 mM Na-Carbonate pH 10 buffer.

Proteophene	Hydrodynamic radius (nm) pH 2	Hydrodynamic radius (nm) pH 10
HS-84-E-E	318	205
HS-84-K-K	119	132
HS-84-V-V	3256	185
HS-84-Y-Y	1562	163
HS-84-E-Y	1053	105
HS-84-Y-E	53	128
HS-84-E-V	1029	312
HS-84-V-E	995	138

the other proteophenes, HS-84-V-V, HS-84-Y-Y, HS-84-E-V, HS-84-V-E and HS-84-E-Y, produced longer lag times in the

autocorrelation function, as well as larger scattering intensities in the acidic environment compared to when exposed to alkaline conditions (Figure 4 and SI, Figure S7).

The longer lag times in the autocorrelation function can be attributed to a decrease in solution dynamics, indicating formation of larger structures in acidic buffer, suggesting that the protonation of the carboxylic groups are beneficial for molecular self-assembly of these proteophenes and a similar observation was recently reported for L- and D- tyrosine functionalized oligothiophenes.^[32] Calculated hydrodynamic radius for the individual proteophenes in the different conditions, using a mass weighted algorithm, further confirmed the presence of larger molecular assemblies in 10 mM Na-Citrate pH 2 buffer for HS-84-V-V, HS-84-Y-Y, HS-84-E-V, HS-84-V-E and HS-84-Y-E, whereas HS-84-E-E, HS-84-K-K and HS-84-Y-E displayed similar hydrodynamic radius in both conditions (Table 3). Hence, the position and the chemical nature of the amino acid functionality greatly affects the structural organization of the proteophene. Tyrosine (HS-84-Y-Y and HS-84-E-Y) or valine (HS-84-V-V and HS-84-E-V) substituents in the α -position of the conjugated oligothiophene backbone appear to have a positive impact on the π -stacking, leading to larger structures, whereas charged amino acid substitutions, lysine or glutamate (HS-84-K-K or HS-84-E-E) in the same position seems to favour smaller structures. Moreover, proteophenes, HS-84-E-Y and HS-84-Y-E, with the same amino acid functionalities but in different positions displayed different behaviour in acid conditions. Thus, a molecular interplay between the amino acid functionalities of the β -positions and the amino acid functionalities of the terminal α -positions could also influence the structural rearrangement of the proteophenes in acidic conditions. Overall, DLS measurements confirmed that some proteophenes formed larger self-assembled aggregates in 10 mM Na-Citrate pH 2 buffer and that alkaline conditions produces smaller aggregates which is in line with observations from the photo-physical characterization.

Structural Characterization of the Proteophenes

In addition to the DLS measurements, we next confirmed that several of the oligothiophene derivatives formed larger assemblies in acidic conditions (10 mM Na-Citrate pH 2) by negative stain transmission microscopy (TEM). Granular aggregated material appeared co-deposited with fiber structures for HS-84-E-E, HS-84-V-V, HS-84-E-Y, HS-84-V-E and HS-84-E-V (Figure 5), while HS-84-Y-Y appeared mostly granular. Certain long fibers were found for HS-84-V-V and HS-84-E-Y. Extensive amounts of fibers were formed for HS-84-E-E, HS-84 V-E and HS-84-E-V, where the latter formed entangled networks of fibers. These observations correlated rather well with the strong ICD signal from HS-84-E-E, HS-84 V-E and HS-84-E-V at pH 2 (Figure 3). For HS-84-K-K and HS-84-Y-E, the proteophenes showing the smallest hydrodynamic radius (Table 3), no large assemblies could be observed by TEM. Overall, the observations by TEM agreed with the photophysical characterization and the DLS measurements, as well as confirmed that that the chemical nature, as well as

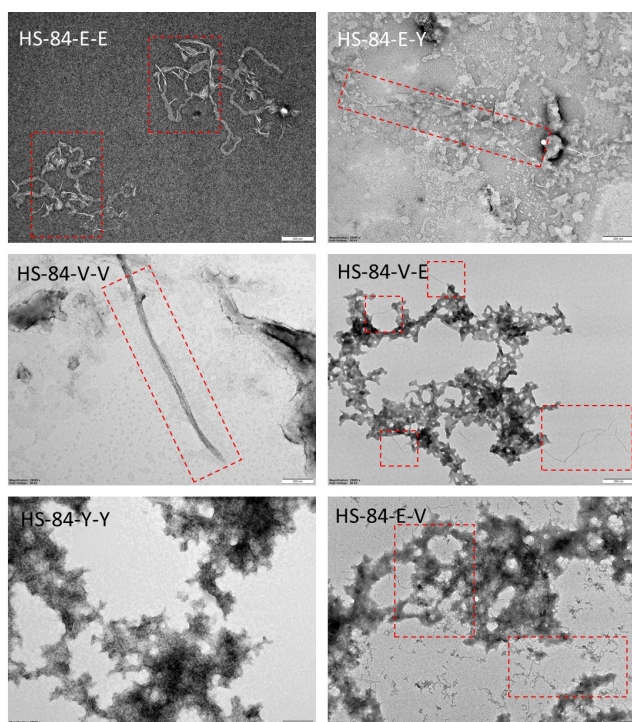


Figure 5. Transmission electron micrographs of proteophene aggregates formed in acidic conditions. Red squares mark areas containing fiber morphologies. Negative stained with uranyl acetate (2%) imaged at 25000x. Scale bars (bottom right in each figure) represent 200 nm.

well as the position of the amino acid substituents, have a large impact on the molecular architecture of the self-assembled proteophene structures.

Correlation between amino acid substituents and the chiroptical/structural characteristics of the proteophenes

When comparing the pattern of amino acid substituents along the pentameric thiophene backbone with the chiroptical and structural properties of the ligands in acidic conditions (Table 4),

several correlations between the chemical composition of the ligand and the ICD, as well as the structural properties, can be observed. Firstly, the shape of the cotton effect seems to be determined by the amino acid functionality in the β -position of distinct thiophene moieties. Proteophenes having glutamate (E) or valine (V) residues in the β -positions exhibit a positive (short wavelengths)/negative (longer wavelengths) signature independent of the amino acid functionality in the α -positions. Likewise, both the proteophenes with tyrosine (Y) in the β -position, HS-84-Y-Y and HS-84-E-Y, displayed negative/positive ICD signatures. Hence, in accordance with the theoretical calculation suggesting that the ICD signals from oligothiophenes originates from conformer populations with distinct dihedral angles between the thiophene rings,^[32] distinct dihedral angles into the forms of cis-minus (M) or cis-plus (P) seems to be governed by the amino acid substituents in the β -positions. Secondly, the ICD signal was most intense for the proteophene, HS-84-E-E, having glutamate (E) in both the α - and β -positions, as well as the proteophenes, HS-84-E-V and HS-84-V-E, having the combination of valine (V) and glutamate (E) in the respective positions and these three proteophenes also displayed extensive amount of fibrillar structures when analyzed by TEM. In contrast, the protophenes, HS-84-Y-E and HS-84-E-Y, having the combination of tyrosine (Y) and glutamate (E) in the respective positions showed rather weak ICDs, as well as granular aggregates (HS-84-E-Y) or no observable structures (HS-84-Y-E). Furthermore, HS-84-Y-Y, having glutamate (Y) in both the α - and β -positions showed similar ICD and TEM characteristics as HS-84-E-Y. From a biomolecular perspective, π -stacking interactions between heterocycles and the aromatic amino acid side chains, such as tyrosine, are highly important and contributes to protein stabilization, as well as to the specific binding of a variety of molecules to proteins.^[48–54] Thus, for the proteophenes have tyrosine (Y) substituents, π -stacking interactions between different thiophene residues along the conjugated backbone with tyrosine residues of adjacent oligothiophene chains are plausible and such interactions might in fact explain the observed differences in chiroptical and structural characteristics for HS-84-E-V and HS-84-V-E versus HS-84-E-Y and HS-84-Y-E, as well as for HS-84-E-E versus HS-84-Y-Y.

Table 4. Correlation between amino acid substituents with the chiroptical properties and structural characteristics of the proteophenes in 10 mM Na-Citrate pH 2 buffer.

α -amino acid	β -amino acid	Cotton effect signature ^b	ICD intensity (mdeg) ^a	TEM structure
E	E	pos/neg	30.5	Granular aggregates and extensive amount of fibers
K	K	neg/pos	10.5	No observable structures
V	V	pos/neg	1.9	Granular aggregates and fibers
Y	Y	neg/pos	4.1	Mostly granular aggregates
E	Y	neg/pos	4.2	Granular aggregates and fibers
Y	E	pos/neg	1.2	No observable structures
E	V	pos/neg	56.8	Granular structures and extensive amount of fibers
V	E	pos/neg	21.5	Granular structures and extensive amount of fibers

^a Calculated from the positive Cotton effect. ^b Short wavelength/longer wavelength.

Similar to the tyrosine substituted proteophenes, HS-84-V-V having valine (V) substituents in both the α - and β -positions also displayed a relatively weak ICD intensity, suggesting that only hydrophobic amino acid substituents are unfavourable for generating a proteophene with efficient chiroptical properties. When the valines in the α - or β -positions were replaced by charged polar glutamates, HS-84-E-V and HS-84-V-E, the ICD intensity increased substantially, and more fibrillary structures were also observed by TEM. Hence, proteophenes having negatively charged polar amino acids in combination with hydrophobic amino acid moieties seem to render well-structured materials with excellent chiroptical properties. At pH 2, there are most likely a mixture of unprotonated and protonated carboxylic groups (pK_a α -COOH=2.3 and pK_a γ -COOH=4.07) so the glutamate residues can act as both hydrogen bond donors and acceptors, suggesting that hydrogen bonding is a key factor for the formation of these self-assembled materials under acid conditions. This argument is also supported by the observations for HS-84-E-E, since this proteophene also displayed a rather high ICD intensity, as well as extensive amount of fibrillar structures. In contrast, as mentioned above, the other proteophenes with glutamate functionalities, HS-84-E-Y and HS-84-Y-E, showed lower ICDs, indicating that π -stacking interactions between different thiophene residues along the conjugated backbone with tyrosine residues might be a stronger driving force for self-assembly than the hydrogen bonding possibilities obtained from the glutamate residues.

The proteophene, HS-84-K-K, functionalized with lysine residues in both the α - and β -positions also showed a relatively high ICD signal, and in contrast to the other proteophenes, the ICD was similar under both acid and alkaline conditions (Figure 3 and Table 4). In addition, no larger assemblies could be observed with DLS or TEM and the photophysical characterization also suggested that HS-84-K-K display fully dissolved single oligothiophene chains in both the conditions. From a chemical perspective, the lysine side functionalities of this proteophene have a zwitter-ionic character and the α -COOH groups, as well as the ϵ -amine groups can also act as both hydrogen donors and acceptors. Thus, the lysine functionalities offer a variety of possibilities for electrostatic interactions and hydrogen bonding patterns that will govern the chiroptical properties and the structure of the ligand. Interestingly, similar single chain ICD signatures has also been observed from polythiophenes with zwitter-ionic side-chain functionalities,^[23,24] as well as an optically inactive anionic polythiophene mixed with a cationic peptide,^[10] suggesting that an acid-base complexation between anionic carboxyl groups and cationic amine groups can induce a similar chiroptical and structural behavior as observed for HS-84-K-K.

Conclusions

In conclusion, amino acid functionalized pentameric oligothiophenes, denoted proteophenes, were shown to exhibit distinct pH-induced photophysical properties, optical activity, and

structural organization. These parameters were highly influenced by the respective substitution patterns of amino acids along the thiophene backbone, as well as the chemical nature of the amino acid side chain functionality. We foresee that our findings will aid in the chemical design of chiral optoelectronic proteophenes that can be employed as optoelectronic materials for a variety of applications within organic electronics and bioelectronics.

Supporting Information

Full experimental details, as well as supporting figures and schemes are given in the Supporting Information.

Acknowledgements

Our work was supported by the Swedish Research Council (Grants No. 2016-00748 and 2019-04405).

Conflict of Interests

The authors declare no conflict of interest.

Data Availability Statement

The data that support the findings of this study are available from the corresponding author upon reasonable request.

Keywords: oligothiophenes · chirality · induced circular dichroism · self-assembly · chiro-optical aggregates

- [1] M. Lemaire, D. Delabouglise, R. Garreau, A. Guy, J. Roncali, *J. Chem. Soc. Chem. Commun.* **1988**, 658–661.
- [2] D. Kotkar, V. Joshi, P. K. Ghosh, *J. Chem. Soc. Chem. Commun.* **1988**, 917–918. >
- [3] J. Roncali, R. Garreau, F. Delabouglise, F. Garnier, M. Lemaire, *Synth. Met.* **1989**, 28, 341–348.
- [4] M. Andersson, P. O. Ekeblad, T. Hjertberg, O. Wennerström, O. Inganäs, *Polymer* **1991**, 32, 546–548.
- [5] M. M. Bouman, E. E. Havinga, R. A. J. Janssen, E. W. Meijer, *Mol. Cryst. Liq. Cryst.* **1994**, 256, 439–448.
- [6] M. M. Bouman, E. W. Meijer, *Adv. Mater.* **1995**, 7, 385–387.
- [7] G. Bidan, S. Guillerez, V. Sorokin, *Adv. Mater.* **1996**, 8, 157–160.
- [8] F. Andreani, L. Angiolini, D. Caretta, E. Salatelli, *J. Mater. Chem.* **1998**, 8, 1109–1111.
- [9] K. P. R. Nilsson, J. Rydberg, L. Baltzer, O. Inganäs, *Proc. Natl. Acad. Sci. USA* **2003**, 100, 10170–10174.
- [10] K. P. R. Nilsson, J. Rydberg, L. Baltzer, O. Inganäs, *Proc. Natl. Acad. Sci. USA* **2004**, 101, 11197–11202.
- [11] R. Selegård, Z. Rouhbakhsh, H. Shirani, L. B. G. Johansson, P. Norman, M. Linares, D. Aili, K. P. R. Nilsson, *Macromolecules* **2017**, 50, 7102–7110.
- [12] L. A. P. Kane-Maguire, G. G. Wallace, *Chem. Soc. Rev.* **2010**, 39, 2545–2576.
- [13] M. Marinelli, L. Angiolini, M. Lanzi, F. Di Maria, E. Salatelli, *Chirality* **2020**, 32, 1361–1376.
- [14] B. M. W. Langeveld-Voss, M. M. Bouman, M. P. T. Christiaans, R. A. J. Janssen, E. W. Meijer, *Polym. Prepr.* **1996**, 37, 499–500.

- [15] B. M. W. Langeveld-Voss, R. A. J. Janssen, M. P. T. Christiaans, S. C. J. Meskers, H. P. J. M. Dekkers, E. W. Meijer, *J. Am. Chem. Soc.* **1996**, *118*, 4908–4909.
- [16] B. M. W. Langeveld-Voss, M. P. T. Christiaans, R. A. J. Janssen, E. W. Meijer, *Macromolecules* **1998**, *31*, 6702–6704.
- [17] B. M. W. Langeveld-Voss, R. A. J. Janssen, E. W. Meijer, *J. Mol. Struct.* **2000**, *521*, 285–301.
- [18] H. Goto, E. Yashima, Y. Okamoto, *Chirality* **2000**, *12*, 396–399.
- [19] E. Yashima, T. Matsushima, Y. Okamoto, *J. Am. Chem. Soc.* **1997**, *119*, 6345–6359.
- [20] E. Yashima, K. Maeda, Y. Okamoto, *Nature* **1999**, *399*, 449–451.
- [21] K. Maeda, S. Okada, E. Yashima, Y. Okamoto, *J. Polym. Sci. Part A* **2001**, *39*, 3180–3189.
- [22] M. Ishikawa, K. Maeda, E. Yashima, *J. Am. Chem. Soc.* **2002**, *124*, 7448–7458.
- [23] K. P. R. Nilsson, M. R. Andersson, O. Inganäs, *J. Phys. Condens. Matter* **2002**, *14*, 10011–10020.
- [24] K. P. R. Nilsson, J. D. M. Olsson, P. Konradsson, O. Inganäs, *Macromolecules* **2004**, *37*, 6316–6321.
- [25] S. Sakurai, H. Goto, E. Yashima, *Org. Lett.* **2001**, *3*, 2379–2382.
- [26] O. Henze, W. J. Feast, F. Gardebien, P. Jonkheijm, R. Lazzaroni, P. Leclere, E. W. Meijer, A. P. H. J. Schenning, *J. Am. Chem. Soc.* **2006**, *128*, 5923–5929.
- [27] S. Schmid, E. Mena-Osteritz, A. Kopyshchev, P. Bäuerle, *Org. Lett.* **2009**, *11*, 5098–5101.
- [28] A. Digennaro, H. Wennemers, G. Joshi, S. Schmid, E. Mena-Osteritz, P. Bäuerle, *Chem. Commun.* **2013**, *49*, 10929–10931.
- [29] N. A. K. Ochs, U. Lewandowska, W. Zajaczkowski, S. Corra, S. Reger, A. Herdlitschka, S. Schmid, W. Pisula, K. Mullen, P. Bäuerle, H. Wennemers, *Chem. Sci.* **2019**, *10*, 5391–5396.
- [30] Z. Guo, Y. Wang, X. Zhang, R. Gong, Y. Mu, X. Wan, *Front. Chem.* **2019**, *7*, 467.
- [31] T. Sanji, N. Kato, M. Tanaka, *Org. Lett.* **2005**, *8*, 235–238.
- [32] M. Bäck, R. Selegård, Y. Todarwal, S. Nyström, P. Norman, M. Linares, P. Hammarström, M. Lindgren, K. P. R. Nilsson, *ChemistryOpen* **2020**, *9*, 1100–1108.
- [33] L. Björk, M. Bäck, L. Lantz, B. Ghetti, R. Vidal, T. Klingstedt, K. P. R. Nilsson, *Chemistry* **2022**, *28*, e202201557.
- [34] A. Åslund, A. Herland, P. Hammarström, K. P. R. Nilsson, B. H. Jonsson, O. Inganäs, P. Konradsson, *Bioconjugate Chem.* **2007**, *18*, 1860–1868.
- [35] A. Åslund, C. J. Sigurdson, T. Klingstedt, S. Grathwohl, T. Bolmont, D. L. Dickstein, E. Glimsdal, S. Prokop, M. Lindgren, P. Konradsson, D. M. Holtzman, P. R. Hof, F. L. Heppner, S. Gandy, M. Jucker, A. Aguzzi, P. Hammarström, K. P. R. Nilsson, *ACS Chem. Biol.* **2009**, *4*, 673–684.
- [36] P. Hammarström, R. Simon, S. Nyström, P. Konradsson, A. Åslund, K. P. R. Nilsson, *Biochemistry* **2010**, *49*, 6838–6845.
- [37] R. A. Simon, H. Shirani, K. O. A. Åslund, M. Bäck, V. Haroutunian, S. Gandy, K. P. R. Nilsson, *Chemistry* **2014**, *20*, 12537–12543.
- [38] H. Hevekerl, J. Wiggenius, G. Persson, O. Inganäs, J. Widengren, *J. Phys. Chem. B* **2014**, *118*, 5924–5933.
- [39] C. Roux, M. Leclerc, *Macromolecules* **1992**, *25*, 2141–2144.
- [40] B. Kim, L. Chen, J. Gong, Y. Osada, *Macromolecules* **1999**, *32*, 3964–3969.
- [41] J. Kim, T. M. Swager, *Nature* **2001**, *411*, 1030–1034.
- [42] J. Sjöqvist, J. Maria, R. A. Simon, M. Linares, P. Norman, K. P. R. Nilsson, M. Lindgren, *J. Phys. Chem. A* **2014**, *118*, 9820–9827.
- [43] H. Yamagata, F. C. Spano, *J. Chem. Phys.* **2012**, *136*, 184901.
- [44] F. C. Spano, C. Silva, *Annu. Rev. Phys. Chem.* **2014**, *65*, 477–500.
- [45] N. J. Hestand, F. C. Spano, *Chem. Rev.* **2018**, *118*, 7069–7163.
- [46] L. Farouil, F. Alary, E. Bedel-Pereira, J.-L. Heully, *J. Phys. Chem. A* **2018**, *122*, 6532–6545.
- [47] K. Rurak, M. Spieles, *Anal. Chem.* **2011**, *83*, 1232–1242.
- [48] S. K. Burley, G. A. Petsko, *Science* **1985**, *229*, 23–28.
- [49] G. B. McGaughey, M. Gagne, A. K. Rappe, *J. Biol. Chem.* **1998**, *273*, 15458–15463.
- [50] R. Chelli, F. L. Gervasio, P. Procacci, V. Schettino, *J. Am. Chem. Soc.* **2002**, *124*, 6133–6143.
- [51] A. S. Wibowo, M. Singh, K. M. Reeder, J. J. Carter, A. R. Kovach, W. Meng, M. Ratnam, F. Zhang, C. E. Dann, *Proc. Natl. Acad. Sci. USA* **2013**, *110*, 15180–15188.
- [52] W. H. Hudson, E. A. Ortlund, *Nat. Rev. Mol. Cell Biol.* **2014**, *15*, 749–760.
- [53] R. Ferreira de Freitas, R. J. Harding, I. Franzoni, M. Ravichandran, M. K. Mann, H. Ouyang, M. Lautens, V. Santhakumar, C. H. Arrowsmith, M. Schapira, *J. Med. Chem.* **2018**, *61*, 4517–4527.
- [54] A. N. Bootsma, A. C. Doney, S. E. Wheele, *J. Am. Chem. Soc.* **2019**, *141*, 11027–11035.

Manuscript received: August 15, 2023

Revised manuscript received: December 1, 2023

Accepted manuscript online: December 18, 2023

Version of record online: January 18, 2024